

## Dynamics and configurational entropy in the Lewis-Wahnström model for supercooled orthoterphenyl

S. Mossa,<sup>1,2</sup> E. La Nave,<sup>1</sup> H. E. Stanley,<sup>1</sup> C. Donati,<sup>2</sup> F. Sciortino,<sup>2</sup> and P. Tartaglia<sup>2</sup>

<sup>1</sup>Center for Polymer Studies and Department of Physics, Boston University, Boston, Massachusetts 02215

<sup>2</sup>Dipartimento di Fisica, INFN and INFN Center for Statistical Mechanics and Complexity, Università di Roma "La Sapienza," Piazzale Aldo Moro 2, I-00185, Roma, Italy

(Received 27 November 2001; published 10 April 2002)

We study thermodynamic and dynamic properties of a rigid model of the fragile glass-forming liquid orthoterphenyl. This model, introduced by Lewis and Wahnström in 1993, collapses each phenyl ring to a single interaction site; the intermolecular site-site interactions are described by the Lennard-Jones potential whose parameters have been selected to reproduce some bulk properties of the orthoterphenyl molecule. A system of  $N=343$  molecules is considered in a wide range of densities and temperatures, reaching simulation times up to 1  $\mu s$ . Such long trajectories allow us to equilibrate the system at temperatures below the mode coupling temperature  $T_c$  at which the diffusion constant reaches values of order  $10^{-10}$   $\text{cm}^2/\text{s}$  and thereby to sample in a significant way the potential energy landscape in the entire temperature range. Working within the inherent structures thermodynamic formalism, we present results for the temperature and density dependence of the number, depth and shape of the basins of the potential energy surface. We evaluate the total entropy of the system by thermodynamic integration from the ideal—noninteracting—gas state and the vibrational entropy approximating the basin free energy with the free energy of  $6N-3$  harmonic oscillators. We evaluate the configurational part of the entropy as a difference between these two contributions. We study the connection between thermodynamical and dynamical properties of the system. We confirm that the temperature dependence of the configurational entropy and of the diffusion constant, as well as the inverse of the characteristic structural relaxation time, are strongly connected in supercooled states; we demonstrate that this connection is well represented by the Adam-Gibbs relation, stating a linear relation between  $\log D$  and the quantity  $1/TS_c$ . This relation is found to hold both above and below the critical temperature  $T_c$ —as previously found in the case of silica—supporting the hypothesis that a connection exists between the number of basins and the connectivity properties of the potential energy surface.

DOI: 10.1103/PhysRevE.65.041205

PACS number(s): 66.10.Cb, 61.43.Fs, 64.70.Pf

### I. INTRODUCTION

Understanding the dynamic and thermodynamic properties of supercooled liquids is one of the more challenging tasks of condensed matter physics (for recent reviews see Refs. [1–4] and references therein). A significant amount of experimental [5–9], numerical [10] and theoretical work [11–15] is being currently devoted to the understanding of the physics of the glass transition and to the associated slowing down of the dynamics. Among the theoretical approaches, an important role has been played by the mode coupling theory (MCT) [11,12], which, interpreting the glass transition as a purely dynamical phenomenon, has constituted a significant tool for the interpretation of both experimental [5,9,16–19] and numerical simulation results [20–22] in weakly supercooled states.

In recent years the study of the topological structure of the potential energy (hyper-) surface (PES) [23,24] and the connection between the properties of the PES and the dynamical behavior of glass-forming liquids has become an active field of research. Building on the inherent structure (IS) thermodynamic formalism proposed a long time ago by Stillinger and Weber [23], the PES can be uniquely partitioned in local basins and properties of the basins explored in supercooled states (average basin depth and basin volume) have been quantified. Studies have mainly focused on two fundamental

questions: (i) which are the basins relevant for the thermodynamics of the system, i.e., which are the basins populated with largest probability? and (ii) which are the topological properties of the regions of the PES actually explored by the system during its dynamics? From this point of view, the PES approach has somehow unified, at least on a phenomenological level, the thermodynamic and dynamic approaches to the glass transition.

Numerical analysis of the PES has shown that trajectories in configuration space can be separated into intrabasin and interbasin components [25,26]. The time scales of the two components become increasingly separated on cooling. The intrabasin motion has been associated with the high-frequency vibrational dynamics, while the structural relaxation ( $\alpha$  relaxation) has been related to the process of exploration of different basins. It has also been shown that on lowering  $T$ , the system populates basins of lower and lower energy [27,28]. The  $T$  dependence of the depth of the typical sampled basins follows a  $1/T$  law [29–31] for fragile liquids, and, for strong liquids, it appears to approach a constant value on cooling [32]. The number of basins  $\Omega$  as a function of the basin depth  $e_{IS}$  has also been recently evaluated for a few models [29,30,32–35], opening the possibility of calculating the so-called configurational entropy  $S_c$  and its  $T$  dependence.  $S_c$ , defined as the logarithm of the number of accessible basins  $S_c \equiv k_B \log \Omega$ , has been successfully com-

pared with theoretical predictions [13,36]. At the same time, the approaches and the techniques developed for the analysis of the PES of structural glasses have spread to the field of disordered spin systems, where similar calculations have been performed [37] and similar conclusions have been reached. The evaluation of  $S_c$  for models of glass-forming liquids allows us to numerically check, in a very consistent way, the relation between  $S_c$  and the systems characteristic time  $\tau$ , proposed by Adam and Gibbs [38], and recently “derived” in a novel way [14]. Numerical support for a relation between the  $T$  dependence of  $S_c$  and the  $T$  dependence of  $\tau$ , although limited to very few models, is providing new physical insight on the connection between thermodynamics and long time dynamical properties. The ideas developed within the inherent structure formalism have also been generalized to out-of-equilibrium conditions where the slow aging dynamics has been interpreted as the process of searching for basins of increasingly deep energy [39–42].

In this paper we study the properties of the PES for a rigid model [Lewis and Wahnström (LW)] of the fragile glass former orthoterphenyl (OTP), first introduced by Lewis and Wahnström [43] and recently revisited by Rinaldi *et al.* [44]. We have studied the properties of the PES in a temperature range in which the diffusion coefficient varies by more than four orders of magnitudes for five different density values. This work attempts to build a bridge between models of more direct theoretical interest, like Lennard-Jones (LJ) and soft spheres, and models which appear to reproduce, even if in a crude way, properties of complex materials. In this respect, orthoterphenyl is the best candidate, being one of the most studied glass-forming liquids [17]. The LW model is a three-sites model, with intermolecular site-site interactions described by the LJ potential. This model is among the simplest models for a nonlinear molecule. The limitation constituted by the fact that it does not take into account the internal molecular degrees of freedom (see [45] for a more realistic model), is overruled by the observation that its simplicity—it can be considered as an atomic LJ with constraints—allows one to reach simulation times of the order of  $\mu s$ . Hence a significant sampling of the PES in a large temperature and density range is possible. Moreover, this model constitutes an ideal bridge between simple atomic models and molecular models, being possible to treat it under several approximations [44].

The paper is structured as follows: In Sec. II we briefly recall the main results of the IS formalism. In Sec. III we show the calculation of the configurational entropy as a difference between the total entropy and the vibrational entropy. In Sec. IV we give some numerical details. We present our results in Sec. V, which is divided into subsections detailing the calculation of the total entropy by thermodynamical integration from the ideal gas state, the study of the vibrational properties of the PES, and the calculation of the configurational entropy. In the end we study the link between configurational entropy and the diffusion constant, investigating the validity of the Adam-Gibbs equation. In Sec. VI we finally discuss our results and we draw some conclusions. In Appendix A we report the analytical calculation of the total entropy

of a system of LW molecules in the noninteracting “ideal gas” limit.

## II. INHERENT STRUCTURE THERMODYNAMICS FORMALISM

In this section we briefly review the IS formalism in the  $NVT$  ensemble [23,46], the extension to the  $NPT$  ensemble poses no particular problems [23]. This formalism has become an important tool in the numerical analysis of classical models since it is numerically possible to calculate in a very precise way the inherent structures (defined as the local minima of the PES) and hence compare the theoretical predictions with the numerical results. Given an instantaneous configuration of the system, a steepest descent path along the potential energy hypersurface defines the closest IS.

In the IS formalism, the partition function of a system is written as a sum over all the PES basins. Basins of given IS energy contribute non-negligibly to the total sum if their IS energy is very low, if their volume is very large, and/or if they are highly degenerate, i.e., several basins are characterized by this IS energy. This corresponds to partitioning the phase space in the local energy minima of the PES and their basins of attraction. Such a partition is motivated by the fact that in supercooled states, the typical time scales of the intrabasin and interbasin dynamics differ by several orders of magnitude and hence the separation of intrabasin and interbasin variables becomes meaningful.

In the  $6N$ -dimensional configuration space, the partition function  $Z$  for a system of  $N$  rigid molecules can be written as

$$Z = \frac{(\Lambda_x \Lambda_y \Lambda_z)^N}{\lambda^{3N}} \int d\mathbf{q}^N \exp[-V(\mathbf{q}^N)/k_B T], \quad (1)$$

where  $\mathbf{q}^N$  denotes the positions and orientations of the molecules,  $V(\mathbf{q}^N)$  is the potential energy,  $I_\mu$ , where  $\mu=x,y,z$  are the principal moments of inertia of the molecule,  $\Lambda_\mu \equiv (2\pi I_\mu k_B T)^{1/2}/h$ , and  $\lambda \equiv h(2\pi m k_B T)^{-1/2}$  is the de Broglie wavelength.

Let  $\Omega(E_{IS})$  denote the number of minima with energy  $E_{IS}$ , and  $f(T, E_{IS})$  the average free energy of a basin with basin depth  $E_{IS}$ .  $f(T, E_{IS})$ , which takes into account both the kinetic energy of the system and the local structure of the basin with energy  $E_{IS}$ , is defined by

$$f(T, E_{IS}) \equiv -k_B T \ln \left[ \frac{(\Lambda_x \Lambda_y \Lambda_z)^N}{\lambda^{3N}} \frac{1}{\Omega(E_{IS})} \times \sum_{\text{basins}} \int_{R_{\text{basin}}} d\mathbf{q}^N \exp[-(V - E_{IS})/k_B T] \right], \quad (2)$$

where  $R_{\text{basin}}$  is the configuration volume associated with the specific basin. The partition function can then be rewritten as a sum over all basins in configurational space, i.e.,

$$Z = \sum_{E_{IS}} \Omega(E_{IS}) \exp\left(-\frac{E_{IS} + f(T, E_{IS})}{k_B T}\right) \\ = \sum_{E_{IS}} \exp\left(-\frac{-TS_c(E_{IS}) + E_{IS} + f(T, E_{IS})}{k_B T}\right), \quad (3)$$

where the configurational entropy  $S_c(E_{IS})$  has been defined as

$$S_c(E_{IS}) \equiv k_B \ln[\Omega(E_{IS})]. \quad (4)$$

In the thermodynamic limit, the free energy of the liquid can be calculated using

$$F[e_{IS}(T)] = e_{IS}(T) + f[T, e_{IS}(T)] - TS_c[e_{IS}(T)], \quad (5)$$

where  $e_{IS}(T)$ , the average value of the IS energy at temperature  $T$ , is the solution of the saddle point equation

$$1 + \frac{\partial f}{\partial E_{IS}} - T \frac{\partial S_c}{\partial E_{IS}} = 0. \quad (6)$$

The liquid free energy expression Eq. (5) has a clear interpretation. The first term in Eq. (5) takes into account the average energy of the PES minimum visited, the second term describes the volume of the corresponding basin of attraction and the kinetic energy, and the third term is a measure of the multiplicity of the basin.

It can be rigorously shown [31,46,29] that, if the density of state  $\Omega(E_{IS})$  is Gaussian, and if the basins have approximately the same shape or are, to a good degree, harmonic, the important relation holds,

$$e_{IS}(T) \propto \frac{1}{T}. \quad (7)$$

On lowering  $T$ , basins with lower  $E_{IS}$  energies and lower degeneracy are populated, i.e., both  $e_{IS}$  and  $S_c$  decrease with  $T$ .

### III. EVALUATION OF THE CONFIGURATIONAL ENTROPY

The Eq. (5) provides a natural starting point for a numerical evaluation of the configurational entropy. Indeed, the free energy  $F(T, V)$  per molecule can be split in the usual way as a sum of an energy and an entropic contribution. Considering Eq. (5) we write

$$F(T) = E(T) - TS(T) \\ = -TS_c(T) + e_{IS}(T) + E_v(T) - TS_v(T), \quad (8)$$

where the index  $v$  indicates the vibrational quantities (intra basin components). In order to evaluate these quantities we calculate the basin free energy as the free energy of  $6N-3$  independent harmonic oscillators [34] plus a contribution that takes into account the basin anharmonicities. Then we can write

$$E(T) = \left(6 - \frac{3}{N}\right) \frac{k_B T}{2} + e_{IS}(T) + U_{\text{anh}}(T), \quad (9)$$

$$S(T) = S_v(T) + S_c(T) = S_{\text{harm}}(T) + S_{\text{anh}}(T) + S_c(T), \quad (10)$$

and

$$S_{\text{harm}} = \left(6 - \frac{3}{N}\right) - \frac{1}{N} \sum_{n=1}^{6N-3} \ln\left[\frac{\hbar \omega_n(T)}{k_B T}\right], \quad (11)$$

where the frequencies  $\omega_n$  are the square root of the eigenvalues of the Hessian matrix calculated in the inherent structures.

Thus, the total entropy is the sum of two contributions:  $S_c(T)$  which accounts for the multiplicity of basins of depth  $e_{IS}(T)$ , and  $S_v(T)$  which accounts for the ‘‘volume’’ of the basins. The last equations give us, in a very transparent way, the physical meaning of the partition of the PES; moreover, they provide us with a very efficient way to calculate the configurational entropy as a difference between the total energy of the system and the vibrational entropy.

The total entropy  $S$  can be evaluated via thermodynamic integration, starting from a known reference point. Every variation of total entropy can be generally written as the sum of variation along isochores and isotherms in the form

$$\Delta S = \Delta S_V + \Delta S_T. \quad (12)$$

Then the change of entropy along an isochore between two temperatures  $\bar{T}$  and  $T$  is

$$\Delta S_V = S(V, T) - S(V, \bar{T}) = \int_{\bar{T}}^T \frac{dT'}{T'} c_v(T') \quad (13)$$

and the change along an isotherm between two volumes  $\bar{V}$  and  $V$  is

$$\Delta S_T = S(V, T) - S(\bar{V}, T) \\ = \frac{1}{T} \left[ E(V, T) - E(\bar{V}, T) + \int_{\bar{V}}^V d\bar{V} P(\bar{V}, T) \right]. \quad (14)$$

In the present case, to evaluate the total entropy of the liquid we start from the known expression of the ideal gas of LW molecules, reviewed in the Appendix. To evaluate the basin free energy  $f(T, e_{IS}(T))$ , we select as a reference point the free energy of  $(6N-3)$  independent harmonic oscillators (whose distribution of frequencies can be calculated evaluating the eigenvalues of the Hessian matrix evaluated in the IS structure) and add corrections to take into account the basin anharmonicities. The harmonic contribution to the entropy is given by Eq. (11).

Assuming that the anharmonic contribution is independent from the basin depth, the anharmonic corrections to the entropy at  $T$  can be calculated integrating the quantity  $dU_{\text{anh}}/T$ , where  $U_{\text{anh}}$  is implicitly defined in Eq. (9), from  $T=0$  to  $T$  [see Eq. (13)].

TABLE I. Densities, volumes, and simulation box lengths calculated.

$k$	$\rho_k$ (g/cm <sup>3</sup> )	$V_k$ (nm <sup>3</sup> )	$L_k$ (nm)
1	1.036	126.647	5.022
2	1.060	123.883	4.985
3	1.083	121.120	4.948
4	1.108	118.356	4.910
5	1.135	115.593	4.871

#### IV. NUMERICAL DETAILS

The LW *OTP* molecule [43] is a rigid three-site planar isosceles triangle; the length of the two short sides of the triangle is  $\sigma=0.483$  nm and the angle between them is  $\theta=5\pi/12$  (75°). Each site represents an entire phenyl ring of mass  $m=6m_C\approx 78$  amu, where  $m_C$  is the mass of the carbon atom. For each pair of interacting molecules, nine site-site interactions are evaluated according to the site-site interaction potential

$$V(r)=4\epsilon\left[\left(\frac{\sigma}{r}\right)^{12}-\left(\frac{\sigma}{r}\right)^6\right]+\lambda_1+\lambda_2r, \quad (15)$$

where  $r$  is the site-site distance,  $\epsilon=5.276$  kJ/mol,  $\sigma=0.483$  nm,  $\lambda_1=0.461$  kJ/mol and  $\lambda_2=-0.313$  kJ/(mol nm). The parameters of the potential are selected to reproduce some bulk properties of the *OTP* molecule [43] such as the temperature dependence of the diffusion coefficient and the structure. The values of  $\lambda_1$  and  $\lambda_2$  are selected in such a way that the potential and its first derivative are zero at  $r_c=1.2616$  nm. Such a potential is characterized by a minimum at  $r=0.542$  nm of depth  $-4.985$  kJ/mol. The integration time step is 0.01 ps. The shake algorithm is implemented to account for the molecular constraints.

We study a  $(N,V,E)$  system composed by  $N=343$  molecules (1029 LJ interaction sites) at five different densities (see Table I) for several temperatures at each density (Table II). The overall total simulation time, comprising thermalization and production runs at all the thermodynamic points investigated, exceeds 10  $\mu$ s. We carefully check the thermalization of the system at the lowest temperatures. The lengths of the thermalization runs cover a time interval during which each molecule has moved (on average) a few times  $\sigma$ . This time is calculated by monitoring the mean square displacement. We study also the time dependence of the intermediate scattering function  $F(Q_M,t)=\langle\rho_{Q_M}(t)\rho_{Q_M}^*(0)\rangle$ ; here  $Q_M$  is the value of momentum  $Q$  locating the first maximum of the static structure factor  $S(Q)$ . We confirm that this correlation function has decayed to zero during the equilibration time. Moreover, we ensure that no drift in the one-time quantities is observed during the production run. The lengths of the equilibration runs range from a few nanoseconds at the highest temperatures to several hundred nanoseconds at the lowest temperatures. We have been able to equilibrate the system in a  $T$  range over

TABLE II. Temperatures (in K) for which calculations are performed.

$\rho_1$	$\rho_2$	$\rho_3$	$\rho_4$	$\rho_5$
170	190	230	280	320
185	200	240	300	340
190	210	260	320	360
195	230	280	340	380
210	250	300	360	400
220	280	320	380	420
240	300	340	400	440
260	320	360	420	460
280	340	380	440	480
300	360	410	460	530
			480	

which the diffusion constant changes from  $10^{-6}$  to  $10^{-10}$  cm<sup>2</sup>/s, i.e., over four orders of magnitude.

After the thermalization run, the production run takes place. The length of each run is always several times longer than the estimated relaxation time. This allows us to collect, for each thermodynamic point, a set of configurations which are to a good extent uncorrelated from one another.

Two additional simulations are performed to connect the range of densities and temperature studied with the ideal gas reference point. The system at density  $\rho_4$  is simulated for temperatures ranging from 280 to 5000 K to evaluate the  $T$  dependence of the potential energy. A second set of simulations at constant  $T$  ( $T=5000$  K) in the volume range  $10^2-10^5$  nm<sup>3</sup> is performed to calculate the *excess* pressure (i.e., the pressure beyond the ideal gas contribution).

To calculate the inherent structures visited in equilibrium we perform conjugate gradient minimizations to locate the closest local minima on the PES. We use a tolerance of  $10^{-15}$  kJ/mol in the total energy for the minimization. For each thermodynamical point we minimize at least 100 configurations and we diagonalize the Hessian matrix of at least 50 configurations to calculate the density of states. The Hessian is calculated choosing for each molecule the center of mass and the angles associated with rotations around the three principal inertia axis as coordinates.

Error bars have been calculated for all the simulation results points presented in the paper [47]. Due to the length of the production runs, several times longer than the relaxation times, only configurations sufficiently uncorrelated have been used to calculate the different observables. The error bars have then been calculated using the standard relation for calculating errors. We show the error bars only when the amplitude of the error is larger than the size of the symbol used for the data point.

## V. RESULTS

### A. Dependence of the total entropy on $T$ and $\rho$

To estimate the total entropy for the model we proceed in three steps as shown in Fig. 1. The thermodynamic path has been chosen to avoid the liquid-gas first order line.

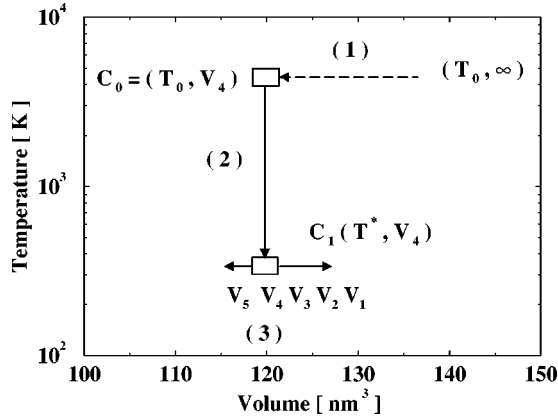


FIG. 1. Thermodynamic integration paths used to calculate the total entropy at the thermodynamical points of interest starting from the ideal—noninteracting—gas state. Details are given in the text.

(1) Integration along the isotherm  $T_0 = 5000$  K from  $(T_0, V = \infty)$  (perfect gas) to  $(T_0, V_4 = 118.356 \text{ nm}^3)$ , corresponding to point  $C_0$  in Fig. 1. The ideal gas contribution to the total entropy is discussed in the Appendix. The entropy at  $C_0$  can be calculated as

$$S(T_0, V_4) - S_{id}(T_0, V_4) = \frac{U(T_0, V_4)}{T_0} + \int_{\infty}^{V_4} \frac{dV}{T_0} P_{ex}(V, T_0), \quad (16)$$

where  $P_{ex}$  is the pressure that exceeds the pressure of the ideal gas, i.e., the contribution to the pressure due to the interaction potential and  $U$  is the system potential energy. The values of the pressure  $P_{ex}(T = T_0, V, N = 343)$  as a function of  $V$  are reported in Fig. 2(a).  $P_{ex}(T = T_0, V, N = 343)$  has been fit using the virial expansion

$$P_{ex}(T = T_0, V, N = 343) = \sum_{k=1}^4 a_k V^{-(k+1)}. \quad (17)$$

The  $a_k$  values are reported in Table III, from which we estimate the first virial coefficient at  $T_0$

$$B_2(T_0) = a_1 / (k_B T_0 N^2) = 0.596 \text{ nm}^3. \quad (18)$$

In Fig. 2(b) we plot the potential energy as a function of volume along the  $T = T_0$  isotherm.

The total entropy at the reference point  $C_0$  is  $S(C_0) = 294.8 \text{ J}/(\text{mol K})$ , resulting from the sum of three contributions

$$S_{id}(C_0) = 339.03 \text{ J}/(\text{mol K}), \quad (19)$$

$$= \int_{\infty}^{V_4} \frac{dV}{T_0} P_{ex}(V, T_0) = -44.9 \text{ J}/(\text{mol K}), \quad (20)$$

and

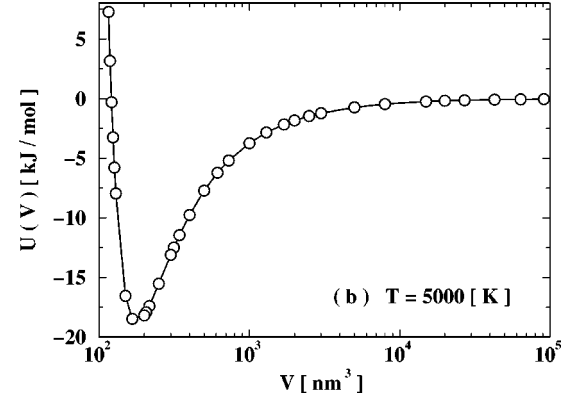
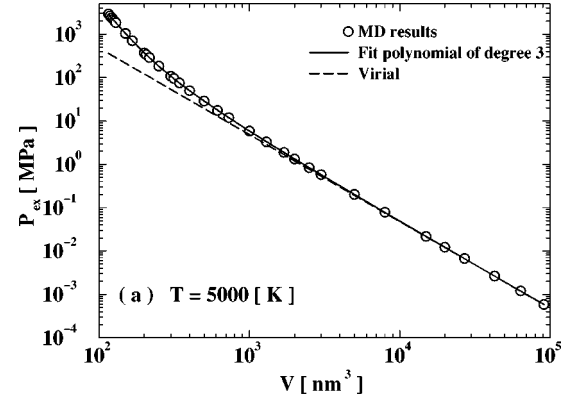


FIG. 2. (a) Excess pressure at  $T = 5000$  K as a function of volume. The open circles are the MD results. The dashed line is the first term of the virial expansion to the excess pressure; the solid line is a third order polynomial fit to the entire set of data. (b) Potential energy at  $T = 5000$  K as a function of volume.

$$\frac{U(C_0)}{T_0} = 0.64 \text{ J}/(\text{mol K}). \quad (21)$$

(2) Integration along the isochore  $V = V_4$  from  $T_0$  to  $T^* = 380$  K, corresponding to point  $C_1$  in Fig. 1. To evaluate the entropy along this isochore we use

$$S(T^*, V_4) = S(T_0, V_4) + 3R \log(T^*/T_0) + \int_{T_0}^{T^*} \frac{dT}{T} \frac{\partial U(V_4, T)}{\partial T}. \quad (22)$$

TABLE III. Fitting coefficients for the excess pressure as a function of  $1/V$  at  $T = 5000$  K and at  $T = 380$  K.

$i$	$a_i$ (MPa nm $^{3(i+1)}$ )	$p_i^*$ (MPa nm $^{3(i+1)}$ )
1	$4835.96272 \times 10^3$	15943.2
2	$1000.53765 \times 10^6$	-256.591
3	$9654.69470 \times 10^6$	1.1745
4	$3873.87001 \times 10^{10}$	-0.00111551

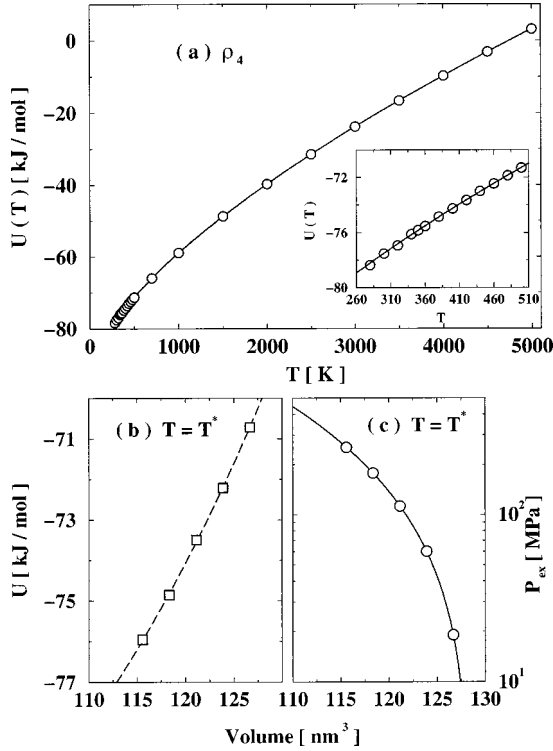


FIG. 3. (a) Integration step 2. Potential energy (open circles) at the density  $\rho_4$  in the entire temperature range considered; the solid line is the fit of the data to Eq. (23). The inset shows the lowest temperature region in order to stress the accuracy of the fit. (b) and (c) Integration step 3. Potential energy (b) and pressure (c).

Figure 3 (a) shows the potential energy for the  $V=V_4$  isochore. To calculate the integral in Eq. (22), we fit the potential energy using the functional form which best interpolates the calculated points

$$U(V_4, T) = u_0 + u_1 T^{3/5} + u_2 T, \quad (23)$$

obtaining the values  $u_0 = -94.405, u_1 = 0.533, u_2 = 0.00183$  (energy in kJ/mol).

The total entropy at the reference point  $C_1$  is  $S(C_1) = 191.8$  J/(mol K), resulting from the sum of three contributions:

$$S(C_0) = 308.6 \text{ J/(mol K)}, \quad (24)$$

$$3R \log(T/5000) = -64.3 \text{ J/(mol K)}, \quad (25)$$

and

$$\int_{T_0}^{T^*} \frac{dT}{T} \frac{\partial U(V_4, T)}{\partial T} = -52.5 \text{ J/(mol K)}. \quad (26)$$

(3) Integration along the isotherm  $T^*$  from  $V_4$  to a “generic”  $V$ . To determine the total entropy difference for all studied densities we calculate

TABLE IV. Total entropy at five densities for the reference temperature  $T^*$ .

$k$	$S(T^*)$ [J/(mol K)]
1	192.80
2	188.21
3	183.54
4	177.95
5	172.12

$$S(T^*, V) - S(T^*, V_4) = S_{id}(T^*, V) - S_{id}(T^*, V_4)$$

$$+ \frac{1}{T^*} [U(T^*, V) - U(T^*, V_4)] + \int_{V_4}^V \frac{dV'}{T^*} P_{ex}(T^*, V'). \quad (27)$$

Figures 3(b) and 3(c) show, respectively, the potential energy and the excess pressure as a function of volume at  $T=T^*$ . For convenience we fit  $P_{ex}$  with a third order polynomial

$$P_{ex}(T^*, V) = \sum_{k=1}^4 p_k^* V^{k-1}, \quad (28)$$

where the values of the coefficients  $p_k^*$  are given in Table III. The resulting total entropy at  $T^*$  for all studied densities is reported in Table IV. These values are used as reference entropies for the  $T$  dependence of  $S$ . For each of the studied isochores, we calculate the  $T$  dependence of the total entropy according to Eq. (22). In this low  $T$  range, the potential energy is very well represented by the Rosenfeld-Tarazona law [48]

$$U(V, T) = U_0(V) + \alpha(V) T^{3/5} \quad (29)$$

consistent with what was found for LJ systems. In Fig. 4 we show the temperature dependence of the potential energy at all densities. The best-fit  $U_0(V)$  and  $\alpha(V)$  values are reported in Table V. The calculated total entropies at each considered density are plotted in Fig. 5.

TABLE V. The first two columns are the coefficients for the potential energy  $U(T, V) = U_0(V) + \alpha(V) T^{3/5}$ ; the second two columns are the coefficients for the inherent structures  $e_{IS}(V, T) = A(V) + B(V)/T$ .

$\rho_k$	$U_0$ (kJ/mol)	$\alpha$ (kJ K <sup>-3/5</sup> /mol)	$A$ (kJ/mol)	$B$ (kJ T/mol)
1	-86.30	0.4385	-79.11	-285
2	-88.94	0.4716	-80.14	-436
3	-92.07	0.5231	-81.88	-676
4	-95.23	0.5762	-81.36	-965
5	-96.06	0.5731	-81.89	-1100

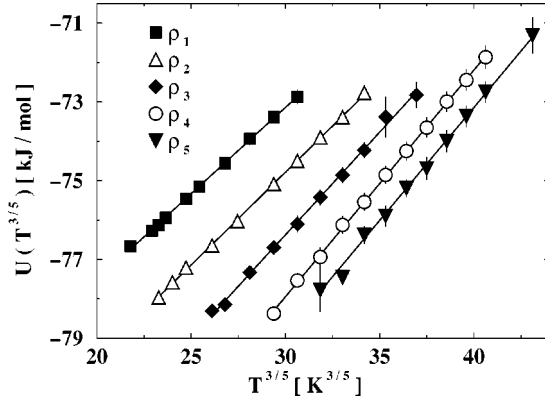


FIG. 4. Potential energies at the different densities as a function of  $T^{3/5}$ . The straight solid lines show the validity of the Rosenfeld-Tarazona law, Eq. (29).

### B. Dependence of the inherent structure energies on $T$ and $\rho$

In Fig. 6 we show the temperature dependence of the energy of the calculated inherent structures together with a fit [according to Eq. (7)] in the form

$$e_{IS}(V, T) = A(V) + \frac{B(V)}{T} \quad (30)$$

The values of the fitting coefficients  $A(V)$  and  $B(V)$  are reported in Table V. On lowering temperature the system populates minima of lower and lower energy. It is worth noting that, in contrast to the case of the actual potential energy, the slope of these curves varies strongly with densities.

From the  $T$  and  $V$  dependence of  $e_{IS}$  the anharmonic potential energy can be calculated according to Eq. (3). Figure 7 shows  $U_{\text{anh}}(T)$  for two densities (symbols). We also show a cubic extrapolation (solid lines) in the form of

$$U_{\text{anh}}(T) = c_2 T^2 + c_3 T^3. \quad (31)$$

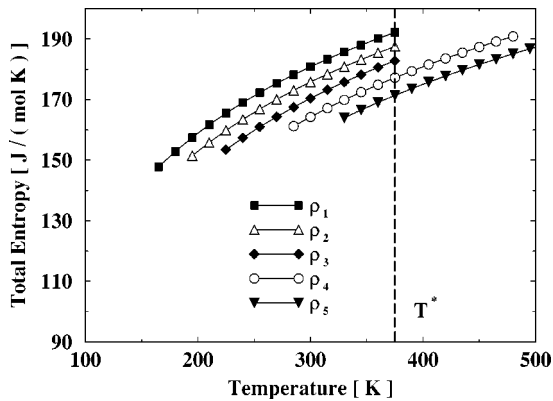


FIG. 5. Temperature dependence of the total entropy as calculated by thermodynamic integration from the ideal gas reference state. Only points in the temperature range where MD measurements have been performed are shown. The reference temperature  $T^* = 380$  K is also shown (dashed line).

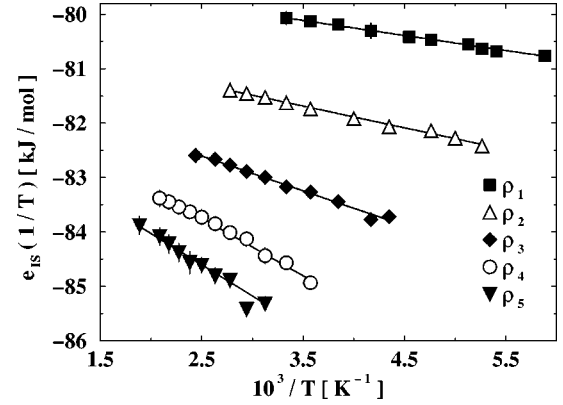


FIG. 6. Energies of the inherent structures at the different densities as a function of  $1/T$ . The straight lines confirm the validity of Eq. (30) in the entire temperature range considered.

As shown in Fig. 7, the anharmonic contribution is rather small, in agreement with previous findings for the LJ model. For this reason, the low signal to noise level does not allow a well-defined characterization of the  $c_2$  and  $c_3$  values. To decrease the number of free parameters, we consider  $c_2$  to be volume independent, and we fit simultaneously, according to Eq. (31),  $c_2$  and the  $V$  dependence of  $c_3$ . As we will show in the following, the anharmonic contribution to the entropy is much smaller than the harmonic one and hence the choice of  $c_2$  and  $c_3$  does not affect significantly the resulting configurational entropy estimate.

### C. Density of states and vibrational harmonic entropy

In this section we study the shape of the basins by investigating the properties of the density of states and we calculate the vibrational harmonic entropy. In Figs. 8(a) and 8(b) we show the temperature and density dependence of the density of state, namely the histogram of the square root of the eigenvalues of the Hessian calculated for the inherent structures. The distribution is characterized by only one peak, not showing any clear separation between translational and rota-

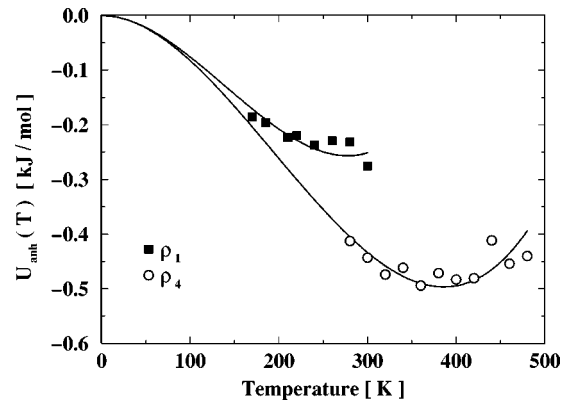


FIG. 7. Anharmonic contributions to the energies, at the two indicated densities, together with the appropriate cubic fit, Eq. (31). This contribution is integrated to directly calculate the anharmonic contribution to the vibrational entropy.

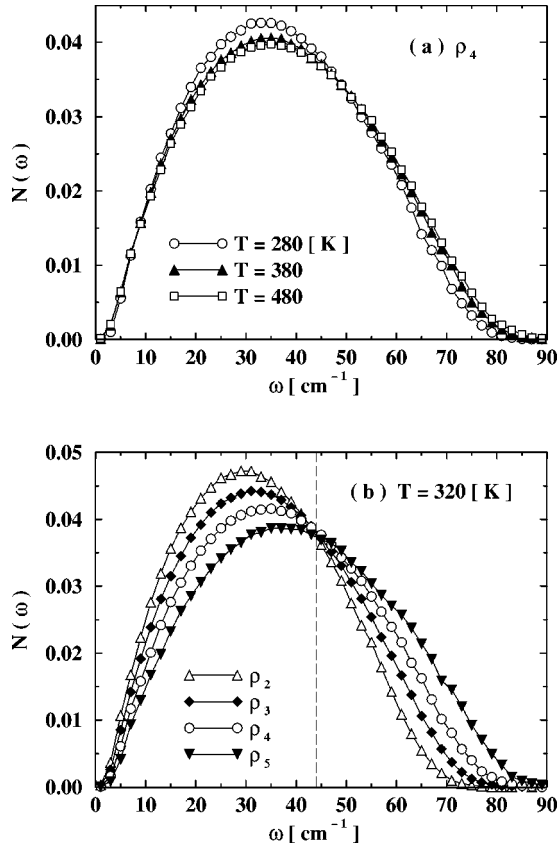


FIG. 8. (a) Density of states at fixed density  $\rho_4$  at the three indicated temperatures. This quantity is the histogram of the square root of the eigenvalues of the Hessian calculated for the inherent structures. (b) Density dependence of the density of state at fixed temperature  $T=320$  K. The dashed line indicates the isosbestic frequency  $\omega^* \approx 44$   $\text{cm}^{-1}$  at which all the curves intersect. The relevance of this feature is discussed in the text.

tional dynamics; the width of the distribution increases on increasing temperature. The position of the maximum is found to be to a good extent independent of temperature; at variance it increases with density as the width does. These features show that the LW PES basins have shapes that are function of the energy depth and of the density.

It is worth noticing one particular feature of Fig. 8(b); all the curves cross at a value of the frequency  $\omega^* \approx 44$   $\text{cm}^{-1}$ . The presence of this isosbestic frequency (in analogy with the well-know isosbestic frequency observed in the Raman spectrum of water [49]) supports the possibility that a two-state model [50] may provide a reasonable description of the change of the density of states with temperature and, correspondingly, of the change of the density of states with the basin depth.

In Figs. 9(a) and 9(b) we plot the quantity  $N^{-1} \sum_{k=1}^{6N-3} \log(\omega_k/\omega_0)$  as a function of  $T$  and of the  $e_{IS}$ , respectively. The scale frequency  $\omega_0$  is chosen as 1  $\text{cm}^{-1}$ . This quantity is an indicator of the average curvature of the basins and, being a sum of logarithms, is very sensitive to the spectrum tails. As shown in Fig. 9(a)  $N^{-1} \sum_{k=1}^{6N-3} \log(\omega_k/\omega_0)$

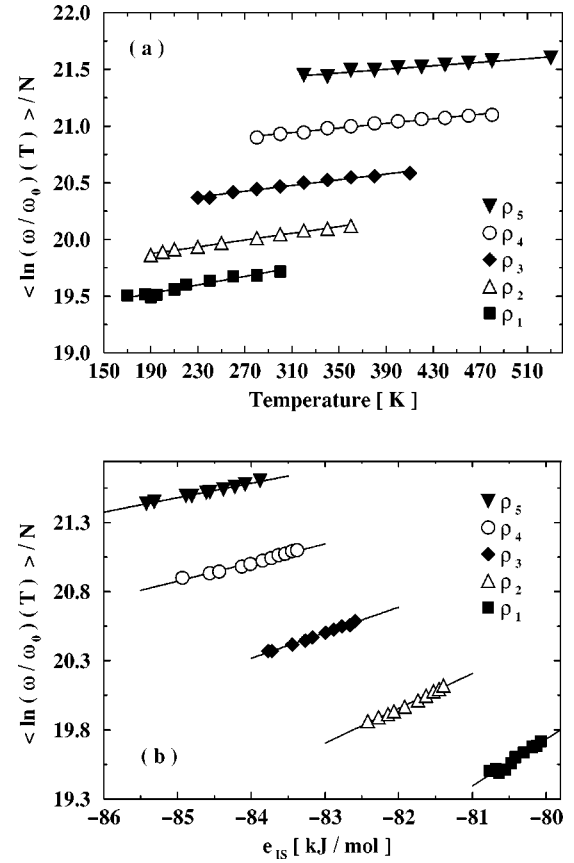


FIG. 9. (a) Temperature dependence of the average basin curvatures  $N^{-1} \sum_{k=1}^{6N-3} \log(\omega_k/\omega_0)$ ; this quantity, being a sum of logarithms, is very sensitive to the spectrum tails.  $\omega_0 = 1$   $\text{cm}^{-1}$  sets the frequency scale. (b) Relation between the energy of the inherent structures and the average basin curvatures. The straight lines confirm the correlation between shape and depth of the inherent structures accessed by the system.

increases with temperature along isochores and increases with density along isotherms.

As noted previously for the LJ [51,29] and for the simple-point charge extended (SPC/E) model for water [30], the dependence of  $N^{-1} \sum_{k=1}^{6N-3} \log(\omega_k/\omega_0)$  from  $e_{IS}$  can be well approximated by a linear dependence, i.e.,

$$\frac{1}{N} \sum_{k=1}^{6N-3} \ln \left[ \frac{\hbar \omega_n(T)}{k_B T_0} \right] = a(V) + b(V) e_{IS}(T), \quad (32)$$

TABLE VI. Coefficients of the fit to the form  $N^{-1} \sum_{k=1}^{6N-3} \log(\omega_k/\omega_0) = a(V) + b(V) e_{IS}(T)$ .

$\rho_k$	$a(V)$	$b(V)$ (mol/kJ)
1	47.1	0.342
2	41.2	0.259
3	36.5	0.192
4	32.1	0.132
5	28.9	0.869

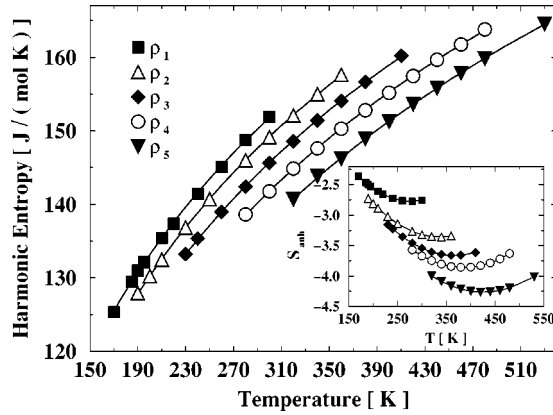


FIG. 10. Main panel: Harmonic contribution to the vibrational entropy as calculated from the eigenvalues of the Hessian for the inherent structures. Inset: Anharmonic contribution to the vibrational entropy as calculated by integration of the anharmonic contribution to the potential energy, as discussed in the text.

where  $T_0$  defines the  $T$  scale ( $T_0 = 1$  K). The values of the coefficients  $a(V)$  and  $b(V)$  are reported in Table VI. This dependence indicates that deeper and deeper basins have larger and larger volumes (their average frequency being smaller). The fact that basins of different depths have different volumes introduces an important contribution to Eq. (6) since the term  $\partial f / \partial e_{IS}$  is different from zero. The implication of this nonzero contribution has been discussed recently in Refs. [29,51,52].

In Fig. 10 we show the harmonic contribution to the entropy as calculated from Eq. (11). This contribution is obviously increasing with temperature and along isotherms increases decreasing density. The lines are interpolations of the data using the fits of Fig. 9.

#### D. Vibrational anharmonic entropy

Integration of the anharmonic energy  $U_{anh}$ , obtained from Eq. (9) according to Eq. (13), gives directly the anharmonic contribution to the entropy. For the LW case,  $U_{anh}$  is described by the polynomial in  $T$  of Eq. (31), and we obtain

$$S_{anh}(T) = 2c_2T + \frac{3}{2}c_3T^2. \quad (33)$$

The inset of Fig. 10 shows the anharmonic contribution to the vibrational entropy as calculated by integrating the anharmonic contribution to the potential energy. This contribution is negative showing that, in the range of densities and temperatures studied, the leading anharmonic contribution acts in the direction to decrease the volume of the basin.

#### E. The configurational entropy

In Fig. 11 we plot the configurational entropy calculated subtracting the vibrational (sum of the harmonic and anharmonic terms) from the total entropy for the five studied isochores. As expected the degeneracy of basins increases on

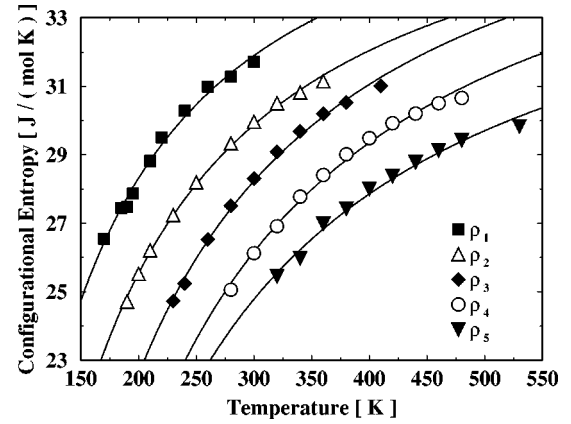


FIG. 11. Volume and temperature dependence of the configurational entropy  $S_c$  calculated as the difference between the total and the vibrational entropy. Solid lines are interpolations of the calculated points to Eq. (34).

lowering density, in agreement with the evidence that a glass transition may be induced along an isothermal path by progressively increasing the pressure. Considering Eqs. (10), (11), (30), (32), and (33), the configurational entropy can be described in the entire density and temperature range considered by means of the functional form

$$S_c(T) = S(T) - \left(6 - \frac{3}{N}\right) + a(V) + b(V) \left[ A(V) + \frac{B(V)}{T} \right] - 2c_2T - \frac{3}{2}c_3T^2. \quad (34)$$

These curves are plotted in Fig. 11 as solid lines. In the range of temperatures and density studied,  $S_c/R$  per molecule varies from about 4 to 3, a figure not very different from the estimated configurational entropy of orthoterphenyl, based on an analysis of the  $T$  dependence of the measured specific heat [53,54]. We recall that the LW model represents each

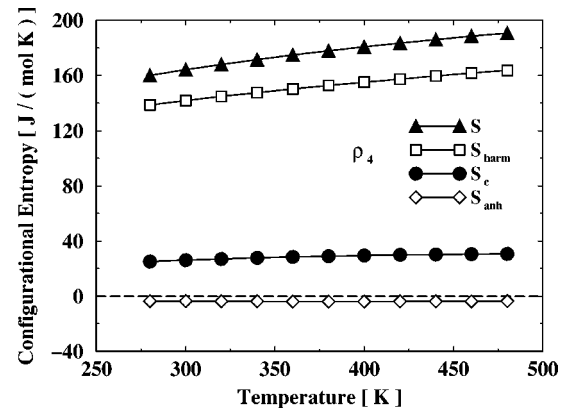


FIG. 12. Temperature dependence of the different contributions to the total entropy (closed triangles) at the fixed selected density  $\rho_4$ : harmonic (open squares), configurational entropy (closed circles), and anharmonic (open diamonds).

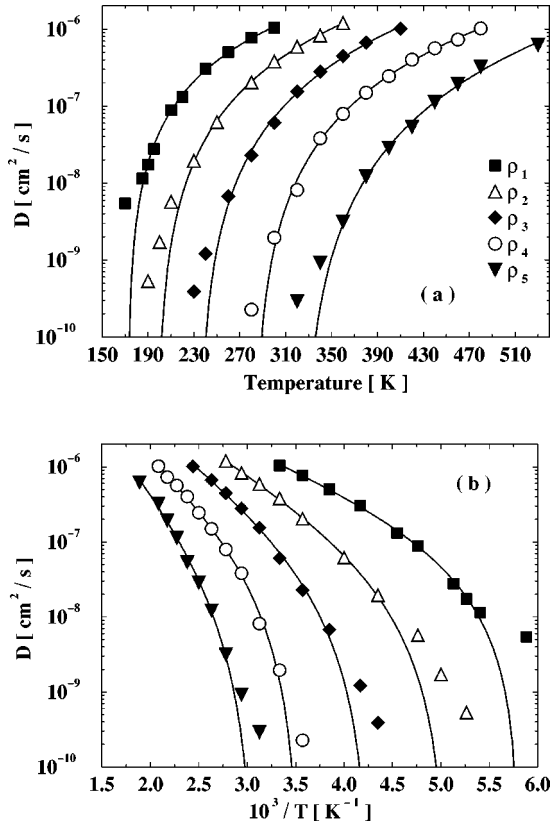


FIG. 13. Diffusion constants together with the corresponding power law fits (solid lines) predicted by the MCT. The breakdown of this prediction and the crossover to an activated dynamics is evident. See text for a discussion of this point. (a) As a function of temperature. (b) As a function of the inverse temperature in order to stress the exponential dependence at the lowest temperatures.

phenyl group as one single interaction site and it does not account for the the molecule flexibility. The similar estimate of  $S_c$  seem to suggest that steric effects are dominant in controlling the configurational entropy. Finally, in Fig. 12 we plot the temperature dependence of all the contributions to the entropy at  $\rho_4$ .

#### F. Diffusion and the Adam-Gibbs relation

In order to investigate the connection between the long time dynamics of the system and the underlying PES, we calculate the center-of-mass diffusion coefficient  $D(T)$  from the mean-square displacement  $\langle r^2(t, T) \rangle$  via the Einstein relation

$$D(T) = \lim_{t \rightarrow \infty} \frac{1}{6t} \langle r^2(t, T) \rangle \quad (35)$$

To guarantee a proper diffusive regime, at all densities simulations are performed until the average mean square displacement is greater than  $0.1 \text{ nm}^2$  at the lowest temperatures and  $10 \text{ nm}^2$  at the highest. The inverse of the diffusion coefficient provides an estimate of the characteristic structural relaxation time of the LW model.

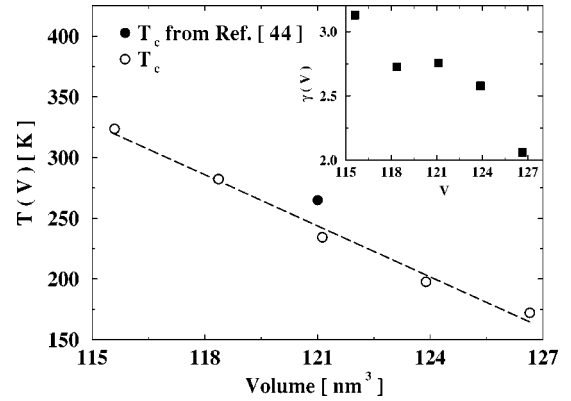


FIG. 14. MCT parameters as calculated from the diffusion constants. Main panel: Critical temperature  $T_c(V)$  (open circles) together with the value calculated in Ref. [44] (closed circle). The dashed line is only a guide for the eye. Inset: Power law exponent  $\gamma(V)$ .

The  $D$  values calculated are shown in Fig. 13. Figure 13(a) shows the dependence on  $T$ , while Fig. 13(b) shows the dependence on  $1/T$ . Figure 13(a) also shows the best fits to the power law

$$D(T) \propto (T - T_c)^\gamma \quad (36)$$

predicted by the ideal MCT in weakly supercooled states. The consistency of the MCT prediction for a wide range of  $D$  values confirms the analysis of Rinaldi *et al.* [44] where explicit ideal MCT calculations were presented and successfully compared with the numerical results along one isobar. Figure 13 shows also that clear deviations from the ideal MCT take place when the diffusion value becomes smaller than  $10^{-8} \text{ cm}^2/\text{s}$ . The representation of  $D$  as a function of  $1/T$  shown in Fig. 13(b) shows that the ideal MCT region is followed by a  $T$  region where new types of processes become effective in controlling the molecular dynamics. These processes, termed hopping processes, transform the ideal MCT divergence of characteristic times into a crossover. In the region of  $D$  values between  $10^{-8} \text{ cm}^2/\text{s}$  and  $10^{-10} \text{ cm}^2/\text{s}$ , limited from below by the present numerical resources, data are consistent with an apparent Arrhenius dependence with parameters which could well become  $T$  dependent if studied in a larger range of  $D$  values [3].

The ideal MCT critical temperatures and  $\gamma$  values, determined by the fit of the  $D$  values to Eq. (36), as a function of density are shown in Fig. 14. The density dependence of  $T_c$  is almost linear. The exponent  $\gamma$  seems to increase on increasing density, but the noise does not allow us to rule out the possibility of a constant value. The filled circle indicates the value of the critical temperature  $T_c = 265 \text{ K}$  determined from an isobaric run in Ref. [44].

We finally study the link between configurational entropy and diffusion coefficient, investigating the validity of the Adam-Gibbs equation. Figure 15 shows  $\log D$  as a function of  $1/(TS_c)$ ; for all studied isochores,  $\log D$  vs  $1/(TS_c)$  is well described by a linear relation, with coefficients which are

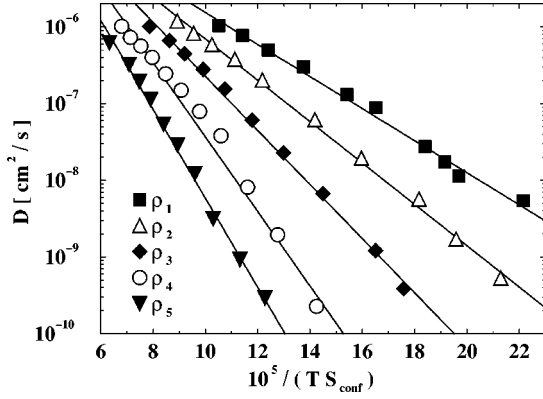


FIG. 15. Test of the Adam-Gibbs relation  $\log D(T) \propto (1/TS_c)$  for five different densities. Note that this linear relation holds both above and below the estimated critical temperatures  $T_c$ .

volume dependent, as previously found for the LJ liquid [29], for the SPC/E model for water [34] and for the BKS model for silica [32].

We note in passing that deviations from linear behavior are observed at large values of  $\log D$ , where intrabasin and interbasin dynamics time scales are no longer separated. At high  $T$ , it has been proposed [55] that entropy—as opposed to configurational entropy—is the relevant thermodynamic quantity controlling dynamics.

## VI. DISCUSSION AND CONCLUSIONS

In this article we have studied systematically the properties of the potential energy surface for a simple three-site rigid model designed to mimic the properties of the fragile glass-forming liquid ortho-terphenyl. The choice of this simple model, which collapses the entire phenyl ring into one interaction site, allows us to run very long trajectories and to study in supercooled states the molecular dynamics up to 1  $\mu s$ , allowing the determination of diffusion coefficients down to  $10^{-10}$   $\text{cm}^2/\text{s}$ .

We have found that, as in the atomic LJ case, by cooling along an isochore, the PES of deeper and deeper energy are explored. The basin volumes are functions of the depth in agreement with previous studies. Using the inherent structure thermodynamic formalism, we have calculated the number of basins of the PES and their depth, in the region of depth values probed by our simulations. As a result, we presented a full characterization of the the temperature and density dependence of the basin depth, degeneracy, and volumes.

These results are used to provide a consistent model for the intrabasin vibrational entropy. This, together with the numerical calculation of the total entropy via thermodynamic integration starting from the ideal gas state, allow us to calculate the configurational entropy—the difference between the total entropy and the vibrational one. This quantity is of primary interest both for comparing with the recent theoretical calculations [13,36] and to examine some of the proposed relation between dynamics and thermodynamics [38,14,56] connecting a purely dynamical quantity like the diffusion coefficient to a purely thermodynamical quantity

( $S_c$ ). To examine such a possibility we compare for five different isochores the  $T$  dependence of  $D$  with the Adam-Gibbs relation. In the entire range of  $T$  and densities studied the Adam-Gibbs relation appears to provide a consistent representation of the dynamics for the LW model.

It is important to observe that a linear relation between  $\log D$  and  $1/(TS_c)$  holds both above and below the ideal MCT critical temperature  $T_c$ , in agreement with a similar finding for the silica case [32]. Recent works based on the instantaneous normal mode technique [57] for several representative models [58–62] provide evidence that above  $T_c$  the system is always located in a region of the PES close to the border between different basins. The number of diffusive directions significantly decreases above  $T_c$  and, if only data above  $T_c$  are considered, the number of diffusive directions would appear to vanish at  $T_c$ . Hence dynamics above  $T_c$  is a dynamics of “borders” between basins and there is no clear reason why such dynamics should be well described by the Adam-Gibbs relation, which focuses on the “number” of basins explored. The observed validity of the AG relation—both above and below  $T_c$ —reported in this manuscript supports the hypothesis that a direct relation exists between the number of basins and their connectivity [60,62]. It is a challenge for future studies to confirm or disprove this hypothesis.

## ACKNOWLEDGMENTS

We thank W. Kob for very useful discussions. We also thank INFN-PRA-HOP, INFN-Iniziativa Calcolo Parallelo, MIURST-COFIN-2000, and NSF Chemistry Program.

## APPENDIX: IDEAL GAS ENTROPY FOR THE LW MODEL

In this appendix we calculate the partition function of a system of  $N$  LW molecules in the noninteracting—ideal gas—case.

The three moments of inertia for the single molecule are

$$I_x = \frac{2}{3} m \sigma^2 \cos^2\left(\frac{\theta}{2}\right) = 1.248 \times 10^{-44} \text{ kg m}^2,$$

$$I_y = 2 m \sigma^2 \sin^2\left(\frac{\theta}{2}\right) = 2.204 \times 10^{-44} \text{ kg m}^2, \quad (\text{A1})$$

and

$$I_z = m \sigma^2 \left[ \frac{2}{3} \cos^2\left(\frac{\theta}{2}\right) + 2 \sin^2\left(\frac{\theta}{2}\right) \right] = 3.452 \times 10^{-44} \text{ kg m}^2.$$

We define the following quantities:

$$\mathcal{A} \equiv \frac{6 \pi m k_B}{h^2}, \quad \mathcal{R}_\mu \equiv \frac{8 \pi^2 k_B I_\mu}{h^2}, \quad (\text{A2})$$

where  $\mu$  denotes  $x$ ,  $y$ , or  $z$ . The translational and rotational partition functions for the single molecule are, respectively [63],

$$\mathcal{Z}_T(T, V) = V\sqrt{(\mathcal{A}T)^3}, \quad (\text{A3})$$

$$\mathcal{Z}_R(T, V) = \frac{1}{2}\sqrt{\pi}\sqrt{\mathcal{R}_x\mathcal{R}_y\mathcal{R}_zT^3}, \quad (\text{A4})$$

so the total partition function for an ideal gas of LW OTP molecules can be expressed as

$$\mathcal{Z}_{id}(T, V, N) = \frac{(\mathcal{Z}_T\mathcal{Z}_R)^N}{N!}. \quad (\text{A5})$$

We approximate  $N! \approx N^N e^{-N}$ . The free energy  $F_{id}$  and the entropy  $S_{id}$  of the non-interacting system then become

$$\begin{aligned} F_{id}(T, V, N) &= -k_B T \ln[\mathcal{Z}_{id}(T, V, N)] \\ &= N \left[ \frac{1}{2} \ln 2 + \ln V \sqrt{\mathcal{A}^3 \mathcal{R}_x \mathcal{R}_y \mathcal{R}_z} \right. \\ &\quad \left. + 3 \ln T - \ln N + 1 \right] \\ S_{id}(T, V, N) &= -\frac{1}{k_B} \frac{\partial}{\partial T} F_{id}(T, V, N) \end{aligned} \quad (\text{A6})$$

$$\begin{aligned} &= N k_B \left\{ 4 + \frac{1}{2} \ln \pi - \ln 2 \right. \\ &\quad \left. + \ln \left[ \frac{V \sqrt{\mathcal{A}^3 \mathcal{R}_x \mathcal{R}_y \mathcal{R}_z}}{N} T^3 \right] \right\} \end{aligned} \quad (\text{A7})$$

where the term  $\ln 2$  is due to the two possible degenerate angular orientations of the molecule [63].

- 
- [1] P.G. Debenedetti and F.H. Stillinger, *Nature (London)* **410**, 259 (2001).
- [2] M. Mézard, in *More is Different*, edited by M. P. Ong and R. N. Bhatt (Princeton University Press, Princeton, NJ, 2001); cond-mat/0110363.
- [3] G. Tarjus and D. Kivelson, e-print cond-mat/0003368.
- [4] P. G. Debenedetti, *Metastable Liquids* (Princeton University Press, Princeton, NJ, 1997).
- [5] G.Q. Shen, J. Toulouse, S. Beaufils, B. Bonello, Y.H. Hwang, P. Finkel, J. Hernandez, M. Bertault, M. Maglione, C. Ecolivet, and H.Z. Cummins, *Phys. Rev. E* **62**, 783 (2000).
- [6] H.Z. Cummins, *J. Phys.: Condens. Matter* **11**, A95 (1999).
- [7] W. Götze, *J. Phys.: Condens. Matter* **11**, A1 (1999).
- [8] C.A. Angell, *Science* **267**, 1924 (1995).
- [9] R. Torre, P. Bartolini, and R.M. Pick, *Phys. Rev. E* **57**, 1912 (1998); A. Taschin, R. Torre, M. A. Ricci, M. Sampoli, C. Dreyfus, and R.M. Pick, *Europhys. Lett.* **56**, 407 (2001).
- [10] K. Binder *et al.*, in *Complex Behaviour of Glassy Systems*, edited by M. Rubi and C. Perez-Vicente (Springer-Verlag, Berlin, 1997).
- [11] W. Götze, in *Liquids, Freezing and the Glass Transition*, edited by J. P. Hansen, D. Levesque, and J. Zinn-Justin (North-Holland, Amsterdam, 1991); W. Götze and L. Sjörge, *Rep. Prog. Phys.* **55**, 241 (1992); W. Götze, *J. Phys.: Condens. Matter* **11**, A1 (1999).
- [12] R. Schilling, in *Disorder Effects on Relaxational Processes* edited by A. Richert and A. Blumen (Springer-Verlag, Berlin, 1994); W. Kob, in *Experimental and Theoretical Approaches to Supercooled Liquids: Advances and Novel Applications*, edited by J. Fourkas *et al.* (ACS Books, Washington, D.C., 1997).
- [13] M. Mézard and G. Parisi, *Phys. Rev. Lett.* **82**, 747 (1999); *J. Phys.: Condens. Matter* **12**, 6655 (2000).
- [14] X. Xia and P.G. Wolynes, *Phys. Rev. Lett.* **86**, 5526 (2001).
- [15] R. Speedy, *J. Phys.: Condens. Matter* **10**, 4185 (1998); **9**, 8591 (1997); **8**, 10907 (1996).
- [16] G. Hinze, David D. Brace, S.D. Gottke, and M.D. Fayer, *Phys. Rev. Lett.* **84**, 2437 (2000).
- [17] M. Kiebel, E. Bartsch, O. Debus, F. Fujara, W. Petry, and H. Sillescu, *Phys. Rev. B* **45**, 10 301 (1992); A. Tölle, H. Schober, J. Wuttke, and F. Fujara, *Phys. Rev. E* **56**, 809 (1997); A. Tölle, H. Schober, J. Wuttke, O.G. Randl, and F. Fujara, *Phys. Rev. Lett.* **80**, 2374 (1998); G. Monaco, D. Fioretto, L. Comez, and G. Ruocco, *Phys. Rev. E* **63**, 061502 (2001).
- [18] J. Gapinski, W. Steffen, and A. Patkowski, *J. Chem. Phys.* **110**, 2312 (1999); A. Aouadi, C. Dreyfus, and M. Massot, *ibid.* **112**, 9860 (2000).
- [19] K.L. Ngai, *J. Chem. Phys.* **110**, 10 576 (1999); R. Casalini, K.L. Ngai, and C.M. Roland, *ibid.* **112**, 5181 (2000); J. Wuttke, M. Ohl, M. Goldammer, S. Roth, U. Schneider, P. Lunkenheimer, R. Kahn, B. Rufflé, R. Lechner, and M.A. Berg, *Phys. Rev. E* **61**, 2730 (2000); M. Goldammer, C. Losert, J. Wuttke, W. Petry, F. Terki, H. Schober, and P. Lunkenheimer, *ibid.* **64**, 021303 (2001).
- [20] T. Gleim, W. Kob, and K. Binder, *Phys. Rev. Lett.* **81**, 4404 (1998).
- [21] L. Fabbian, A. Latz, R. Schilling, F. Sciortino, P. Tartaglia, and C. Theis, *Phys. Rev. E* **60**, 5768 (1999); **62**, 2388 (2000); C. Theis, F. Sciortino, A. Latz, R. Schilling, and P. Tartaglia, *ibid.* **62**, 1856 (2000).
- [22] F. Sciortino and W. Kob, *Phys. Rev. Lett.* **86**, 648 (2001).
- [23] F.H. Stillinger and T.A. Weber, *Phys. Rev. A* **25**, 978 (1982); *Science* **225**, 983 (1984); F.H. Stillinger, *ibid.* **267**, 1935 (1995).
- [24] David J. Wales, *Science* **293**, 2067 (2001).
- [25] T.B. Schröder, S. Sastry, J.C. Dyre, and S.C. Glotzer, *J. Chem. Phys.* **112**, 9834 (2000).
- [26] H. Fynewever, D. Perera, and P. Harrowell, *J. Phys.: Condens. Matter* **12**, A399 (2000).
- [27] S. Sastry, *J. Phys.: Condens. Matter* **12**, 6515 (2000).
- [28] P.S. Shah and C. Chakravarty, *J. Chem. Phys.* **115**, 8784 (2001).
- [29] S. Sastry, *Nature (London)* **409**, 164 (2001).

- [30] F.W. Starr, S. Sastry, E. La Nave, A. Scala, H.E. Stanley, and F. Sciortino, *Phys. Rev. E* **63**, 041201 (2001).
- [31] A. Heuer, *Phys. Rev. Lett.* **78**, 4051 (1997); S. Büchner and A. Heuer, *Phys. Rev. E* **60**, 6507 (1999).
- [32] I. Saika-Voivod, P.H. Poole, and F. Sciortino, *Nature (London)* **412**, 514 (2001).
- [33] F. Sciortino, W. Kob, and P. Tartaglia, *Phys. Rev. Lett.* **83**, 3214 (1999).
- [34] A. Scala, F.W. Starr, E. La Nave, F. Sciortino, and H.E. Stanley, *Nature (London)* **406**, 166 (2000).
- [35] R.J. Speedy, *J. Chem. Phys.* **114**, 9069 (2001).
- [36] B. Coluzzi, G. Parisi, and P. Verrocchio, *Phys. Rev. Lett.* **84**, 306 (2000); B. Coluzzi and P. Verrocchio, *J. Chem. Phys.* **116**, 3789 (2002); B. Coluzzi, M. Mézard, G. Parisi, and P. Verrocchio, *ibid.* **111**, 9039 (1999); B. Coluzzi, G. Parisi, and P. Verrocchio, *ibid.* **112**, 2933 (2000).
- [37] A. Crisanti and F. Ritort, e-print cond-mat/0110259.
- [38] G. Adam and J.H. Gibbs, *J. Chem. Phys.* **43**, 139 (1965).
- [39] W. Kob, F. Sciortino, and P. Tartaglia, *Europhys. Lett.* **49**, 590 (2000).
- [40] S. Mossa, G. Ruocco, F. Sciortino, and P. Tartaglia, *Philos. Mag. B* (to be published).
- [41] A. Scala and F. Sciortino, e-print cond-mat/0106573.
- [42] F. Sciortino and P. Tartaglia, *J. Phys.: Condens. Matter* **13**, 9127 (2001).
- [43] G. Wahnström and L.J. Lewis, *Physica A* **201**, 150 (1993); L.J. Lewis and G. Wahnström, *Solid State Commun.* **86**, 295 (1993); *J. Non-Cryst. Solids* **172-174**, 69 (1994); *Phys. Rev. E* **50**, 3865 (1994); G. Wahnström and L.J. Lewis, *Suppl. Prog. Theor. Phys.* **126**, 261 (1997).
- [44] A. Rinaldi, F. Sciortino, and P. Tartaglia, *Phys. Rev. E* **63**, 061210 (2001).
- [45] S. Mossa, R. Di Leonardo, G. Ruocco, and M. Sampoli, *Phys. Rev. E* **62**, 612 (2000); S. Mossa, G. Ruocco, and M. Sampoli, *ibid.* **64**, 021511 (2001); S. Mossa, G. Monaco, and G. Ruocco, e-print cond-mat/0104265; S. Mossa, G. Monaco, G. Ruocco, M. Sampoli, and F. Sette, *J. Chem. Phys.* **116**, 1077 (2002); S. Mossa, G. Ruocco, and M. Sampoli, e-print cond-mat/0202121.
- [46] F. Sciortino, W. Kob, and P. Tartaglia, *J. Phys.: Condens. Matter* **12**, 1 (2000).
- [47] In this article, all the solid lines found in the figures should be considered as interpolations of the calculated data points (as in the case of the thermodynamic integration section) or as a support to the interpretation of our results in the framework set by theoretical approaches (as in the case of the fit of the diffusion coefficients according to the MCT).
- [48] Y. Rosenfeld and P. Tarazona, *Mol. Phys.* **95**, 141 (1998).
- [49] G.E. Walrafen, M.S. Hokmabadi, and W.H. Yang, *J. Chem. Phys.* **85**, 6964 (1986); see also P. Benassi, V. Mazzacurati, M. Nardone, M. A. Ricci, G. Ruocco, and G. Signorelli, *ibid.* **88**, 4553 (1988).
- [50] C.A. Angell, B.E. Richards, and V. Velikov, *J. Phys.: Condens. Matter* **11**, A75 (1999).
- [51] F. Sciortino and P. Tartaglia, *Phys. Rev. Lett.* **86**, 107 (2001).
- [52] L. M. Martinez and C.A. Angell, *Nature (London)* **410**, 667 (2001).
- [53] F.H. Stillinger, *J. Phys. Chem. B* **102**, 2807 (1998).
- [54] R. Richert and C.A. Angell, *J. Chem. Phys.* **108**, 9016 (1998).
- [55] M. Dzugutov, *Nature (London)* **381**, 137 (1996); *J. Phys.: Condens. Matter* **11**, A253 (1999).
- [56] M. Schulz, *Phys. Rev. B* **57**, 11 319 (1998).
- [57] T. Keyes, *J. Phys. Chem.* **101**, 2921 (1997).
- [58] F. Sciortino and P. Tartaglia, *Phys. Rev. Lett.* **78**, 2385 (1997).
- [59] C. Donati, F. Sciortino, and P. Tartaglia, *Phys. Rev. Lett.* **85**, 1464 (2000).
- [60] E. La Nave, A. Scala, F.W. Starr, F. Sciortino, and H.E. Stanley, *Phys. Rev. Lett.* **84**, 4605 (2000).
- [61] E. La Nave, A. Scala, F.W. Starr, H.E. Stanley, and F. Sciortino, *Phys. Rev. E* **64**, 036102 (2001).
- [62] E. La Nave, H.E. Stanley, and F. Sciortino, *Phys. Rev. Lett.* **88**, 035501 (2002).
- [63] J. E. Mayer and M. G. Mayer, *Statistical Mechanics* (John Wiley & Sons, New York, 1963).